Very Massive and Supermassive Stars: Evolution and Fate

23

Raphael Hirschi

Abstract

This chapter reviews the properties and evolution of very massive stars ($M > 100\,M_{\odot}$) in the context of recent stellar evolution models. At the end of the chapter, we summarize the properties, evolution, and fate of supermassive stars ($M > 10{,}000\,M_{\odot}$). Since very massive stars have very large convective cores during the main sequence phase, their evolution is never far from a chemically homogeneous evolution, even without rotation-induced mixing. Their evolution is thus not so much affected by rotational mixing, but more by mass loss through strong stellar winds. All very massive stars at metallicities close to solar end their life as hydrogen-free Wolf-Rayet stars. At solar metallicity, mass loss is so strong that even if a star is born with several hundred solar masses, it will end its life with less than 50 $M_{\odot}$. This means that their fate will be similar to normal massive stars. At the metallicity of the Large Magellanic Cloud (LMC) and lower, on the other hand, mass loss is weaker and might allow stars to undergo pair-instability supernovae or pulsation pair-instability supernovae. These supernovae are expected to be very rare but very bright and able to explain a subset of slowly evolving super-luminous supernovae. Supermassive stars might be the progenitors of intermediate-mass or super massive black holes or explain anti-correlations between the abundance of specific chemical elements in star clusters. In rare circumstances they might explode due to a general relativistic instability. Supermassive stars formation and their evolution, however, are very uncertain

R. Hirschi (✉)
Astrophysics Group, School of Chemical and Physical Sciences, Keele University, Staffordshire, UK

Kavli Institute for the Physics and Mathematics of the Universe (WPI), University of Tokyo, Kashiwa, Chiba, Japan

UK Network for Bridging Disciplines of Galactic Chemical Evolution (BRIDGCE), Staffordshire, UK
e-mail: r.hirschi@keele.ac.uk

A.W. Alsabti, P. Murdin (eds.), *Handbook of Supernovae*,
https://doi.org/10.1007/978-3-319-21846-5_120

and there is no solid evidence for their existence. If they exist, supermassive stars evolve close to the Eddington limit, and thus their mass loss is probably very strong and makes their fate similar to very massive stars.

Contents

1 Introduction

For many decades, the evolution of very massive stars (VMS: $M > 100\,M_{\odot}$) was considered only in the framework of Pop III stars. Indeed, it was expected that only in metal-free environments could such massive stars be formed, since the absence of dust, an efficient cooling agent, would prevent a strong fragmentation of the proto-stellar cloud (see e.g., Abel et al. 2002a; Bromm et al. 1999). Note, however, that recent star formation simulations find lower-mass stars forming in groups, similarly to present-day star formation (see Greif et al. 2010; Stacy et al. 2010). It came therefore as a surprise when the most metal-poor low-mass stars, likely formed from a mixture between the ejecta of these Pop III stars and pristine interstellar medium, did not show any signature of the peculiar nucleosynthesis of the VMS (Christlieb et al. 2002; Frebel et al. 2005; Heger and Woosley 2002; Umeda and Nomoto 2002). While such observations cannot rule out the existence of these VMS in Pop III generations (their nucleosynthetic signature may have been diluted or erased by the more important impact of stars in other mass ranges), it questions the importance of such objects for understanding the early chemical evolution of galaxies.

As the importance of VMS in the early universe seems to decrease, their importance in the local universe increases. For a long time, observations favoured a present-day upper mass limit for stars around 150 $M_{\odot}$ (Figer 2005; Oey and Clarke 2005), which would mean that very few stars are VMS. Crowther et al. (2010),

however, have reassessed the properties of the brightest members of the R136a star cluster, revealing exceptionally high luminosities. The comparison between main sequence evolutionary models for rotating and non-rotating stars and observed spectra resulted in high current ($\leq$265 $M_{\odot}$) and initial ($\leq$320$M_{\odot}$) masses for these stars. The formation scenarios for these VMS are summarized in Krumholz (2015), and their general properties were reviewed in the recent review book on VMS (Vink 2015).

The above observations triggered a new interest in the evolution of VMS. However, since VMS are so rare, only a few of them are known, and we have to rely on stellar evolution models in order to study their properties and evolution. In this chapter, the evolution of VMS will be discussed based on stellar evolution models calculated using the Geneva stellar evolution code (Eggenberger et al. 2007) including the modifications implemented to follow the advanced stages as described in Hirschi et al. (2004). Models at solar ($Z = 0.014$), Large Magellanic Cloud (LMC, $Z = 0.006$), and Small Magellanic Cloud (SMC, $Z = 0.002$) metallicities will be presented (see Yusof et al. 2013, for full details about these models). These models will also be compared to models of normal massive stars calculated with the same input physics at solar metallicity ($Z = 0.014$) presented in Ekström et al. (2012) and Georgy et al. (2012) as well as their extension to lower metallicities (Georgy et al. 2013).

In Sect. 2, we briefly review the most important stellar evolution model ingredient for VMS, i.e., mass loss. The general properties and early evolution of VMS are presented in Sect. 3. WR stars from VMS are described in Sect. 4. The late evolution and possible fates of the VMS are the subject of Sect. 5. The evolution and fate of supermassive stars are summarized in Sect. 6. A summary and conclusions are given in Sect. 7.

2 Stellar Evolution Models and Mass Loss Prescriptions

The evolution of VMS is similar enough to more common massive stars that the same stellar evolution codes can be used to study their evolution and corresponding nucleosynthesis. Stellar evolution models require a wide range of input physics ranging from nuclear reaction rates to mass loss prescriptions. The main equations governing the evolution of stars as well as their physical ingredients are reviewed in Kippenhahn and Weigert (1990) and Yusof et al. (2013). In this section, we review mass loss since it plays a key role for the evolution of VMS. The reader is referred to the population synthesis study for VMS by Schneider et al. (2014) to see the effects of binarity on VMS.

2.1 Mass Loss

Mass loss strongly affects the evolution of very massive stars as we shall describe below. We recall here the different mass loss prescriptions used in stellar evolution calculations and how they relate to each other.

On the hot side of the Hertzsprung-Russell diagram (HRD), the mass loss driving mechanism (line driving) is generally well understood, and there are both theoretical and empirical mass loss prescriptions. For O-type massive stars, the theoretical prescription for radiative line-driven winds from Vink et al. (2001) is generally used, which compare rather well with observations (Crowther et al. 2010; Muijres et al. 2011). In stellar evolution simulations, the stellar wind is not simulated self-consistently and a criterion is used to determine when a star becomes a WR star. Usually, a star is considered to become a WR when the surface hydrogen mass fraction, X_s, becomes inferior to 0.3 (sometimes when it is inferior ot 0.4) and the effective temperature, $\log(T_{\rm eff})$, is greater than 4.0. The mass loss rate used during the WR phase depends on the WR subtype. For the eWNL phase – when $0.3 > X_s > 0.05$ – Gräfener and Hamann (2008) derived a new theoretical recipe (in the validity domain of this prescription, which usually covers most of the eWNL phase). In many cases, the WR mass loss rate of Gräfener and Hamann (2008) is lower than the rate of Vink et al. (2001) and the latter is a better choice to use in stellar evolution simulations. For the eWNE phase (when $0.05 > X_s$ and the ratio of the mass fractions of $(^{12}\mathrm{C}+ {}^{16}\mathrm{O})/{}^{4}\mathrm{He} < 0.03$) and WC/WO phases (when $(^{12}\mathrm{C}+ {}^{16}\mathrm{O})/{}^{4}\mathrm{He} > 0.03$), the corresponding prescriptions of Nugis and Lamers (2000) are used. Note also that both the Nugis and Lamers (2000) and Gräfener and Hamann (2008) mass loss rates account for clumping effects (Muijres et al. 2011). As is discussed below, the mass loss rates from Nugis and Lamers (2000) for the eWNE phase are much larger than in other phases, and thus the largest mass loss occurs during this phase on the hot side of the HRD. In Crowther et al. (2010), the mass loss prescription from Nugis and Lamers (2000) was used for both the eWNL and eWNE phases (with a clumping factor, $f = 0.1$). The models presented in this chapter thus lose less mass than those presented in Crowther et al. (2010) during the eWNL phase.

For cooler parts of the HRD, the driving mechanisms and prescriptions are much more uncertain. Pulsation and dust are thought to play a key role in mass loss in red super giants (RSGs), whereas there are probably continuum-driven winds in luminous blue variable (LBV) stars (Owocki 2015). No extended theoretical prescriptions are available for these phases, only empirical ones. The de Jager et al. (1988) prescription is generally used for parts of the HRD not covered by the above prescriptions.

The metallicity dependence of the mass loss rates is commonly included in the following way. The mass loss rate used at a given metallicity, $\dot{M}(Z)$, is the mass loss rate at solar metallicity, $\dot{M}(Z_\odot)$, multiplied by the ratio of the metallicities to the power of α: $\dot{M}(Z) = \dot{M}(Z_\odot)(Z/Z_\odot)^\alpha$. α is generally set to 0.85 for the O-type phase and WN phase and 0.66 for the WC and WO phases; and for WR stars, the initial metallicity rather than the actual surface metallicity is used in the equation above following Eldridge and Vink (2006). α is generally set to 0.5 for the de Jager et al. (1988) prescription. For rotating models, the mass loss rates can be obtained by applying a correction factor to the radiative mass loss rate as described in Maeder and Meynet (2000).

In the models presented in this chapter, the following prescriptions were used unless otherwise stated. For O-type stars, the prescription for radiative line-driven winds from Vink et al. (2001) was used. For stars in a domain not covered by the Vink et al or WR prescriptions, the de Jager et al. (1988) prescription was applied to models with $\log(T_{\rm eff}) > 3.7$. For $\log(T_{\rm eff}) \leq 3.7$, a linear fit to the data from Sylvester et al. (1998) and van Loon et al. (1999) (see Crowther 2001) was performed. The formula used is given in Eq. 2.1 in Bennett et al. (2012).

3 General Properties and Early Evolution of VMS

3.1 VMS Evolve Nearly Homogeneously

One of the key characteristics of VMS is the fact that they possess very large convective cores during the MS phase. They therefore evolve quasi-chemically homogeneously even if there is no mixing (due, e.g., by rotation) in radiative zones as first discussed in Maeder (1980). To illustrate this last point, Fig. 1 shows the

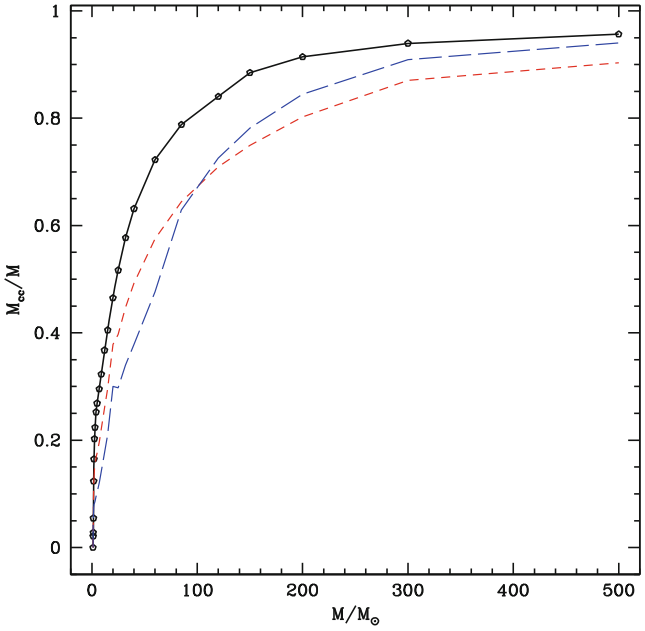

Fig. 1 Mass fraction of the convective core in non-rotating solar metallicity models. This figure and all the following figures are taken from Yusof et al. (2013). Models with initial masses superior or equal to 150 $M_\odot$ are from Yusof et al. (2013). Models for lower initial masses are from Ekström et al. (2012). The continuous line corresponds to the zero-age main sequence (ZAMS); the *short-dashed line* to models when the mass fraction of hydrogen at the center, X_c, is 0.35; and the *long-dashed line* to models when X_c is equal to 0.05

convective core mass fraction for non-rotating massive stars at solar metallicity. It is apparent that the convective cores for masses above 150 $M_\odot$ extend over more than 75% of the total mass of the star, whereas it is less than 50% for typical massive stars.

Figure 2 shows how age, metallicity, and rotation influence this mass fraction. Comparing the *top-left* and *bottom left* panels showing the rotating 150 $M_\odot$ models at solar and SMC metallicities (Z), respectively, we can see that the convective core occupies a very slightly larger fraction of the total mass at SMC metallicity on

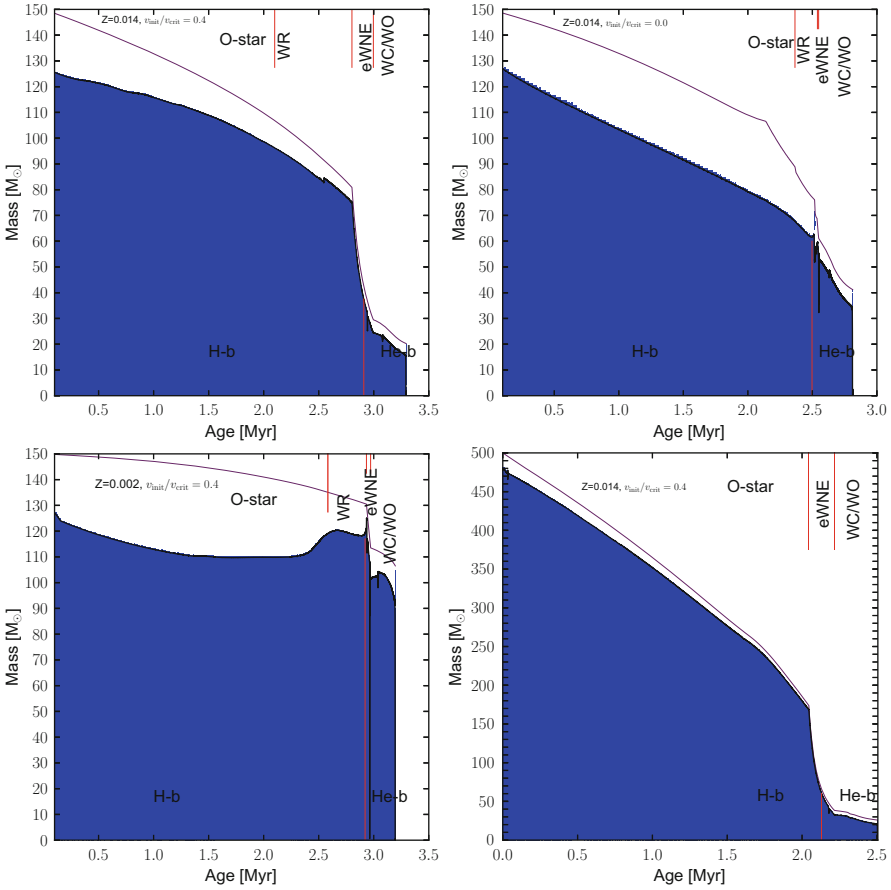

Fig. 2 Structure evolution as a function of age for selected models: solar metallicity 150 $M_\odot$ rotating (*top-left*) and non-rotating (*top-right*) models, rotating SMC metallicity 150 $M_\odot$ model (*bottom left*), and rotating solar metallicity 500 $M_\odot$ model (*bottom right*). The *blue zones* represent the convective regions. The *top solid black line* indicates the total mass of the star, and *vertical red markers* are given for the different phases (O-type, WR = eWNL, eWNE, and WC/WO) at the top of the plots. The transition between H- and He-burning phases is indicated by the *red vertical line* at the bottom of the plots

the ZAMS. As for lower-mass massive stars, this is due to a lower CNO content leading to higher central temperature. This effect is counterbalanced by the lower opacity (especially at very low metallicities) and the net change in convective core size is small. As the evolution proceeds, mass loss is weaker at lower Z and thus the total mass decreases slower than the convective core mass. This generally leads to a smaller fraction of the total mass occupied by the convective core in the SMC models.

We can see the impact of rotation by comparing the rotating (*top-left*) and non-rotating (*top-right*) 150 $M_{\odot}$ models. The convective core size remains higher in the rotating model due to the additional mixing in radiative zones. We can see that rotation-induced mixing can even lead to an increase of the convective core size as is the case for the SMC model (*bottom left*). This increase is typical of quasi-chemically homogeneous evolution also found in studies of normal massive stars (see Yoon et al. 2012, and citations therein). The rotating 500 $M_{\odot}$ model (*bottom right* panel) evolves quasi-homogeneously throughout its entire evolution, even with an initial ratio of the velocity to the critical velocity of 0.4.

These features, very large convective cores and quasi-chemically homogeneous evolution, are key factors governing their evolution as is discussed below.

3.2 Evolutionary Tracks

Figures 3 and 4 show the evolutionary tracks of models with initial masses between 150 and 500 $M_{\odot}$ at various metallicities. Key properties of the VMS models presented in this chapter at the end of H- and He- burning stages are given in Tables 1 and 2, respectively, of Yusof et al. (2013).

Considering first non-rotating solar metallicity stars (see Fig. 3, *left*), the most striking feature is that these massive stars evolve vertically in the HR diagram (HRD) covering only a very restricted range in effective temperature but a very large range in luminosity. This is typical of an evolution mainly governed by mass loss and also by a strong internal mixing (here due mostly to convection as discussed in the previous section).

In normal massive stars, the luminosity of stars increases during the main sequence (MS) phase. For very massive stars, however, the luminosity may decrease slightly during the MS, by about 0.1 dex in the case of the 500 $M_{\odot}$. This is the consequence of very high mass loss rates (of the order of 7×10^{-5} $M_{\odot}$ per year) already at very early evolutionary stages.

Mass loss peels off the envelope, and these VMS enter the WR phase (considered to be when the hydrogen mass fraction at the surface drops below 0.3 in the models) while still burning hydrogen in their core and having nearly the same amount of hydrogen at the center and at the surface, illustrating the nearly homogeneous nature of its evolution (see also Maeder 1980). In this 500 $M_{\odot}$ model, the convective core encompasses nearly 96% of the total mass on the ZAMS (see also Fig. 1).

Further mass loss removes a lot of mass during the WR phase (up to half of the initial mass). This strong mass loss episode translates into the HR diagram by a

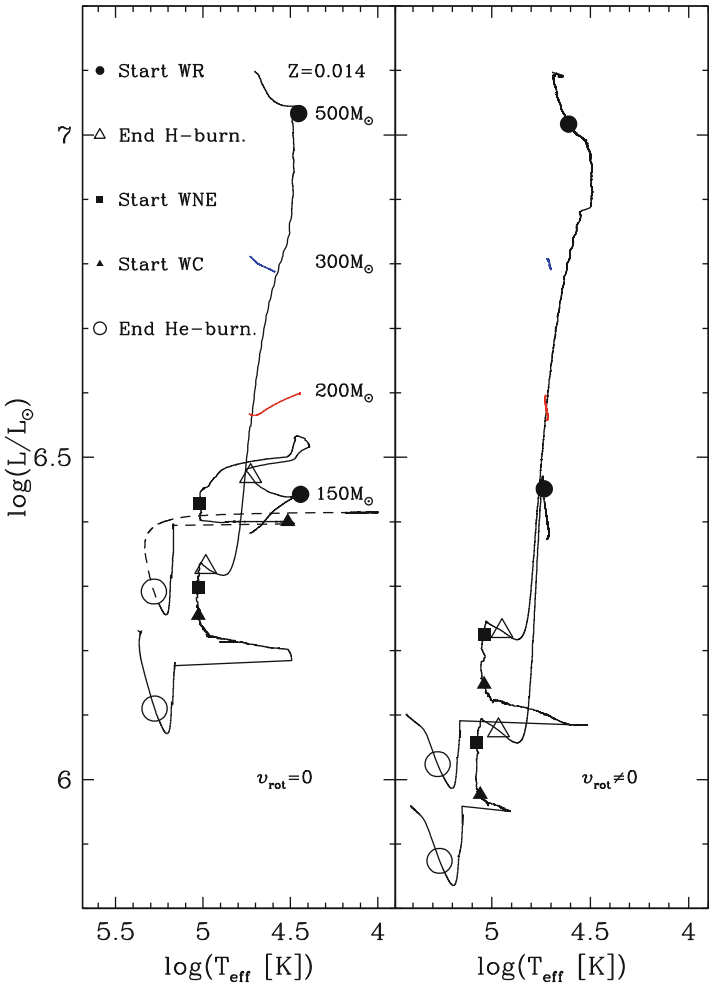

Fig. 3 HR diagram for models between 150 up to 500 $M_{\odot}$ at solar metallicity for non-rotating (*left*) and rotating (*right*) models, respectively. Key stages are indicated along the tracks. Only the first portion (up to start of WR phase) of the tracks for the 200 and 300 $M_{\odot}$ is shown

very important decrease in luminosity. At the end of the MS, the convective core still encompasses a very large fraction of the total stellar mass (80% for the 500 $M_{\odot}$ model).

The core helium burning phase lasts about 10–20% of the MS lifetime as in normal massive stars. At the end of the core He-burning phase, the actual mass of the star is even smaller (only 29.82 $M_{\odot}$ for the 500 $M_{\odot}$ model!).

It is interesting to compare the evolution of the 500 $M_{\odot}$ stellar model with that of the 150 $M_{\odot}$ model. In contrast to the 500 $M_{\odot}$ model, the 150 $M_{\odot}$ increases in luminosity during the MS phase. Looking at the HRD, we see that the O-type

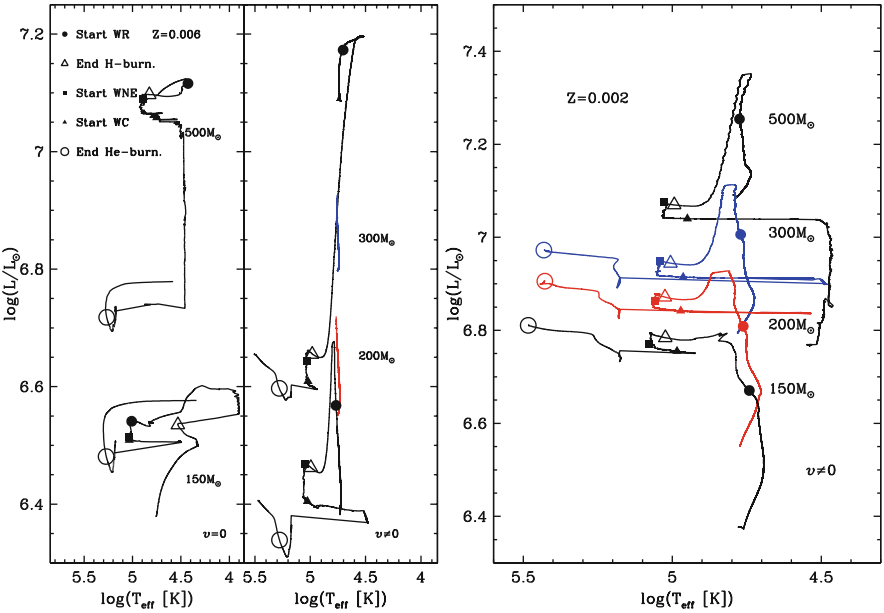

Fig. 4 Same as Fig. 3 for *left*, LMC models ($Z = 0.006$), and *right*, SMC rotating models ($Z = 0.002$)

star phase of the 150 and 500 $M_\odot$ models covers more or less the same effective temperature range. This illustrates the well-known fact that the colors of stars for this mass range do not change much with the initial mass.

When the stars enter into the WR phase, in contrast to the case of the 500 $M_\odot$ where the luminosity decreases steeply, the luminosity of the 150 $M_\odot$ model continues to increase a little. The luminosities of the two models when the hydrogen mass fraction at the surface becomes inferior to 10^{-5} differ by just a little more than 0.1 dex. The effective temperatures are similar. Thus one expects stars from very different initial masses to occupy similar positions in the HRD (the 500 $M_\odot$ star being slightly less luminous than the 150 $M_\odot$ during the WR phase). We note that after the end of the core He-burning phase, the star may evolve to the red and terminate its lifetime around an effective temperature of log $T_{\rm eff}$ equal to 4. This comes from the core contraction at the end of core He-burning, which releases energy and leads to an envelope expansion akin to the expansion of the envelope at the end of the MS (see also Yoshida and Umeda 2011).

The duration of the core H-burning phase of the 150 $M_\odot$ model is not much different from the one of the 500 $M_\odot$ model being 2.5 Myr instead of 2 Myr. The core He-burning lifetime lasts for 0.3 Myr as for the 500 $M_\odot$. The total duration of the WR phase is 0.45 Myr, about half of the WR duration for the 500 $M_\odot$. The 200 $M_\odot$ model has an evolution similar to the 150 $M_\odot$ model, while the 300 $M_\odot$ has an evolution similar to the 500 $M_\odot$.

Let us now consider how rotation changes this picture. The right panel of Fig. 3 shows the evolutionary tracks of the $Z = 0.014$ rotating models in a similar way to the tracks of the non-rotating models in the left panel. The changes brought by rotation are modest because the impact of mass loss dominates over that of rotation and large convective cores already mix material quite far out inside the star. One notes however a few differences between the non-rotating and rotating models. One of the main differences is the fact that the models during their O-type phase evolve nearly vertically when rotation is accounted for. This is the effect of rotational mixing which keeps the star more chemically homogeneous than in the non-rotating case (although, as underlined above, already in models with no rotation, due to the importance of the convective core, stars are never very far from chemical homogeneity). As was the case in the non-rotating tracks, the O-type star phase corresponds to an upward displacement when time goes on in the HR diagram for the 150 $M_{\odot}$ model, while it corresponds to a downward displacement for the more massive models. One notes finally that lower luminosities are reached by the rotating models at the end of their evolution (decrease by about 0.3 dex in luminosity, thus by a factor 2). This comes mainly because the rotating models enter earlier into their WR phase and thus lose more mass.

When the metallicity decreases to Z = 0.006 (see Fig. 4, *left*), as in normal massive stars, tracks are shifted toward higher luminosities and effective temperatures. In this metallicity range, all models evolve upward during their O-type star phase in the HR diagram. This is an effect of the lower-mass loss rates.

As was already the case at solar metallicity, rotation makes the star evolve nearly vertically in the HR diagram. One notes in this metallicity range, much more important effects of rotation than at Z = 0.014, which is also expected, since at these lower metallicity, mass loss rates are smaller and rotation-induced mixing more efficient. We note that most of the decrease in luminosity in the 500 $M_{\odot}$ solar mass model occurs during the WC phase in the Z = 0.006 non-rotating model, while it occurs during the WNL phase in the rotating one. This illustrates the fact that rotational mixing, by creating a much larger H-rich region in the star, tends to considerably increase the duration of the WNL phase. One notes also that while the non-rotating 150 $M_{\odot}$ model enters the WR phase only after the MS phase, the rotating model becomes a WR star before the end of the MS phase.

At the metallicity of the SMC (see Fig. 4, *right*), except for the 500 $M_{\odot}$, the tracks evolve horizontally after the end of the core H-burning phase (triangle in Fig. 4, *right*). The much lower-mass loss rates are responsible for this effect.

3.3 Lifetimes and Mass-Luminosity Relation

Lifetimes for VMS range between 2 and 3 Myr (see Tables 1 and 2 Yusof et al. 2013, for more details). The MS lifetime of non-rotating models at solar metallicity ranges from 2.67 to 1.99 Myr for initial masses ranging from 120 to 500 $M_{\odot}$ showing the well-known fact that VMS have a very weak lifetime dependence on their initial mass.

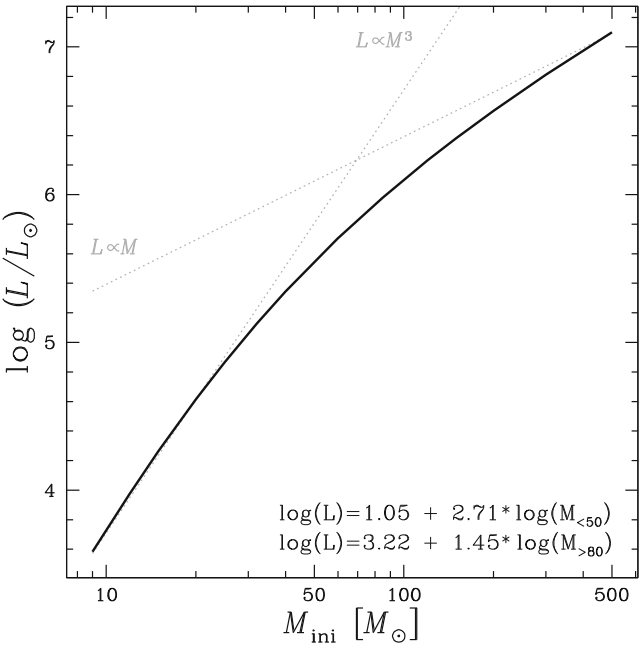

Fig. 5 Mass-luminosity relation on the ZAMS for rotating models at solar metallicity. The formulae in the *bottom right corner* are linear fits for the mass ranges: 9–50 $M_\odot$ and 80–500 $M_\odot$. The non-rotating models have very similar properties on the ZAMS

The mass-luminosity relation on the ZAMS for rotating massive stars at solar composition is shown in Fig. 5. The relation ($L \propto M^\alpha$) is steep for low- and intermediate-mass stars ($\alpha \sim 3$ for $10 < M/M_\odot < 20$) and flattens for VMS ($\alpha \sim 1.3$ for $200 < M/M_\odot < 500$). This flattening is due to the increased radiation pressure relative to gas pressure in massive stars. Since the lifetime of a star is proportional to M/L, we get that for VMS $\tau \propto M/L \propto M^{-0.3}$, which explains the very weak dependence of the lifetime on the mass of the star.

The H-burning (and total) lifetimes of VMS are lengthened by rotation as in lower-mass stars. The difference between the H-burning lifetimes of rotating and non-rotating 150 $M_\odot$ models at solar metallicity is ∼14%. The effects of metallicity on the lifetimes are generally very small. The small differences in total lifetimes are due to different mass loss at different metallicities.

3.4 Mass Loss by Stellar Winds

Mass loss by stellar winds is a key factor governing the evolution of VMS. This comes from the very high luminosities reached by these objects. For example, the luminosity derived for R136a1 is about 10 million times that of our sun.

Table 1 Mass loss properties: total mass of the models at various stages (columns 1–5) and average mass loss rates $\langle \dot{M} \rangle$ during the O-type and eWNE phases (6,7). Masses are in solar mass units and mass loss rates are given in $M_{\odot}\mathrm{yr}^{-1}$

ZAMS	Start eWNL	Start eWNE	Start WC	Final	$\langle \dot{M}_{\mathrm{Vink}} \rangle$	$\langle \dot{M}_{\mathrm{eWNE}} \rangle$
Z = 0.014, $v/v_{crit} = 0.0$						
120	69.43	52.59	47.62	30.81	2.477e-05	3.638e-04
150	88.86	66.87	61.20	41.16	3.274e-05	6.107e-04
200	121.06	91.20	83.85	49.32	4.618e-05	1.150e-03
300	184.27	130.47	52.05	38.15	8.047e-05	8.912e-04
500	298.79	169.50	45.14	29.75	1.736e-04	9.590e-04
Z = 0.014, $v/v_{crit} = 0.4$						
120	88.28	69.54	27.43	18.68	1.675e-05	2.057e-04
150	106.64	80.88	29.49	20.22	2.467e-05	2.640e-04
200	137.52	98.75	31.84	21.93	3.985e-05	3.564e-04
300	196.64	129.10	34.45	23.93	7.559e-05	5.160e-04
500	298.42	174.05	38.30	25.83	1.594e-04	7.901e-04
Z = 0.006, $v/v_{crit} = 0.0$						
120	74.30	57.91	56.91	54.11	2.140e-05	3.272e-04
150	94.18	74.20	71.75	59.59	2.839e-05	5.038e-04
500	332.68	250.64	197.41	94.56	1.304e-04	3.334e-03
Z = 0.006, $v/v_{crit} = 0.4$						
120	100.57	90.78	54.43	39.25	9.429e-06	3.219e-04
150	125.79	111.84	60.75	45.58	1.367e-05	4.418e-04
200	166.81	144.86	66.25	51.02	2.180e-05	6.257e-04
300	247.07	207.10	73.11	54.04	4.166e-05	9.524e-04
500	397.34	315.51	86.10	74.75	9.194e-05	1.685e-03
Z = 0.002, $v/v_{crit} = 0.4$						
150	135.06	130.46	113.51	106.50	6.661e-06	4.485e-04
200	181.42	174.18	137.90	129.21	9.902e-06	6.631e-04
300	273.18	260.81	156.14	149.70	1.730e-05	1.040e-03

For such luminous objects, winds will be very powerful at all evolutionary stages, so while early main sequence VMS are formally O-type stars from an evolutionary perspective, their spectral appearance may be closer to Of or Of/WN at early phases (Crowther et al. 2012).

Table 1 gives the total mass at the start and end of the evolution (note that the models have been evolved beyond the end of core He-burning and usually until oxygen burning, thus very close to the end of their life, see Yusof et al. 2013, for full details) as well as at the transitions between the different WR phases in columns 1 to 5. The average mass loss rates during the O-type and eWNE phases (the phase during which the mass loss rates are highest) are given in columns 6 and 7, respectively.

The evolution of the mass loss rates for various models is shown in Fig. 6. Following the evolution from left to right for the 150 $M_{\odot}$ model at solar metallicity

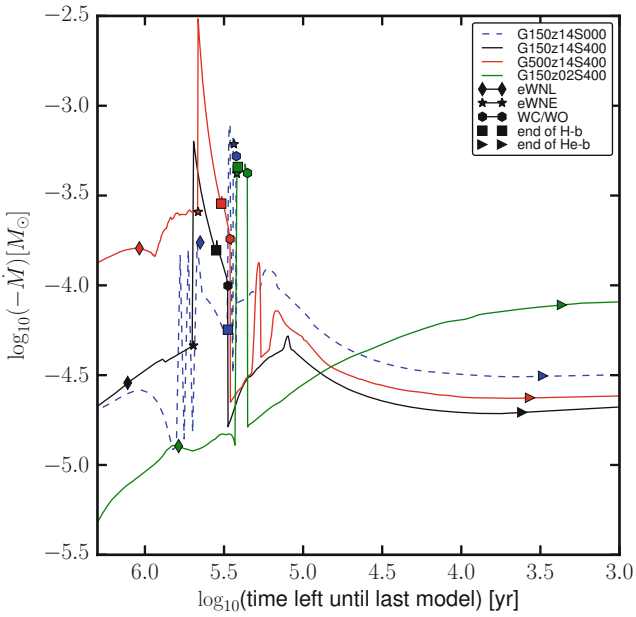

Fig. 6 Evolution of the mass loss rate as a function of time left until last model (log scale) for the rotating 500 $M_\odot$ model (*solid red*), the rotating 150 $M_\odot$ model (*solid black*), the non-rotating (*dashed*) 150 $M_\odot$ model at solar metallicity, and the rotating 150 $M_\odot$ model at SMC metallicity (*solid green*). The diamonds indicate the start of the eWNL phase, stars the start of the eWNE phase, and hexagons the start of the WC/WO phase. The *squares* and *triangles* indicate the end of H-b. and He-b. phases, respectively

(solid black), mass loss rates slowly increase at the start of the O-type phase with mass loss rates between $10^{-5}\,M_\odot\,\mathrm{yr}^{-1}$ (absolute values for the mass loss rates, $-\dot{M}$, are quoted in this paragraph) and $10^{-4.5}\,M_\odot\,\mathrm{yr}^{-1}$. If a bi-stability limit is encountered during the MS phase, as is the case in the non-rotating 150 $M_\odot$ model, mass loss rates can vary significantly over a short period of time and mass loss peaks reach values higher than $10^{-4}\,M_\odot\,\mathrm{yr}^{-1}$. The highest mass loss rate is encountered at the start of the eWNE phase (star symbols) with values in excess of $10^{-3}\,M_\odot\,\mathrm{yr}^{-1}$ (note that the mass loss rate in the non-rotating model has a peak at the end of the H-burning phase due to the star reaching temporarily cooler effective temperatures). Such high mass loss rates quickly reduce the mass and luminosity of the star, and thus the mass loss rate also decreases quickly during the eWNE phase. During the WC/WO phase, mass loss rates are of the same order of magnitude as during the O-type phase.

Comparing the rotating 500 and 150 $M_\odot$ model at solar metallicity (solid black and red), we see that more massive stars start with higher mass loss rates but converge later on to similar mass loss rates since the total mass of the models converges to similar values (see Table 1).

Comparing the SMC and solar metallicity 150 $M_\odot$ rotating models, we can clearly see the metallicity effect during the O-type star phase. During the eWNE phase, mass loss rates are similar, and in the WC/WO, mass loss rates in the SMC model are actually higher since the total mass in that model remained high in contrast with solar metallicity models.

Table 1 also shows the relative importance of the mass lost during the various phases and how their importance changes as a function of metallicity. Even though mass loss is the strongest during the eWNE phase, significant amount of mass is lost in all phases.

3.5 Mass Loss Rates and Proximity to the Eddington Limit

Vink et al. (2011) suggest enhanced mass loss rates (with respect to Vink et al. 2001, used in the models presented here) for stars with high Eddington parameters ($\Gamma_e \geq 0.7$, see Eq. 1 in Vink et al. 2011, for the exact definition of Γ_e) that they attribute to the Wolf-Rayet stage. In order to know whether higher mass loss rates near the Eddington limit could have an impact on the models presented in this chapter, we discuss here the proximity of these models to the Eddington limit.

Figure 7 shows the Eddington parameter, $\Gamma_{\rm Edd} = L/L_{\rm Edd} = \kappa L/(4\pi c GM)$, as a function of the initial mass of our models at key stages. Since the Eddington parameter, $\Gamma_{\rm Edd}$, scales with L/M, the curve for $\Gamma_{\rm Edd}$ also flattens for VMS. The ZAMS values for $\Gamma_{\rm Edd}$ range between 0.4 and 0.6, so well below the Eddington limit, $\Gamma_{\rm Edd} = 1$, and below the limiting value of $\Gamma_e = 0.7$ where enhanced mass loss rates are expected according to Vink et al. (2011).

How does $\Gamma_{\rm Edd}$ change during the lifetime of VMS? Figure 8 presents the evolution of $\Gamma_{\rm Edd}$ for a subset of representative models. The numerical values for each model are given at key stages in Tables 1 and 2 in Yusof et al. (2013). Since $\Gamma_{\rm Edd} \propto \kappa L/M$, an increase in luminosity and a decrease in mass both lead to higher $\Gamma_{\rm Edd}$. Changes in effective temperature and chemical composition affect the opacity and also lead to changes in $\Gamma_{\rm Edd}$.

In rotating models at solar metallicity, $\Gamma_{\rm Edd}$ slowly increases until the start of the eWNE phase. This is mainly due to the increase in luminosity and decrease in mass of the model. At the start of the eWNE phase, mass loss increases significantly. This leads to a strong decrease in the luminosity of the model, and as a result, $\Gamma_{\rm Edd}$ decreases sharply.

During the WC/WO phase, mass loss rates being of similar values as during the O-type star phase, $\Gamma_{\rm Edd}$, increase again gradually.

We can see that, at solar metallicity, $\Gamma_{\rm Edd}$ rarely increases beyond 0.7 even in the 500 $M_\odot$ model. There are nevertheless two interesting cases in which values above 0.7 are reached. The first case is during the advanced stages. At this stage, mass loss does not have much time to change the total mass of the star (it is mostly changes in effective temperature and to a minor extent in luminosity that influence the increase in $\Gamma_{\rm Edd}$). This may nevertheless trigger instabilities resulting in strong mass loss episodes. This may have consequences for the type of SN event that such

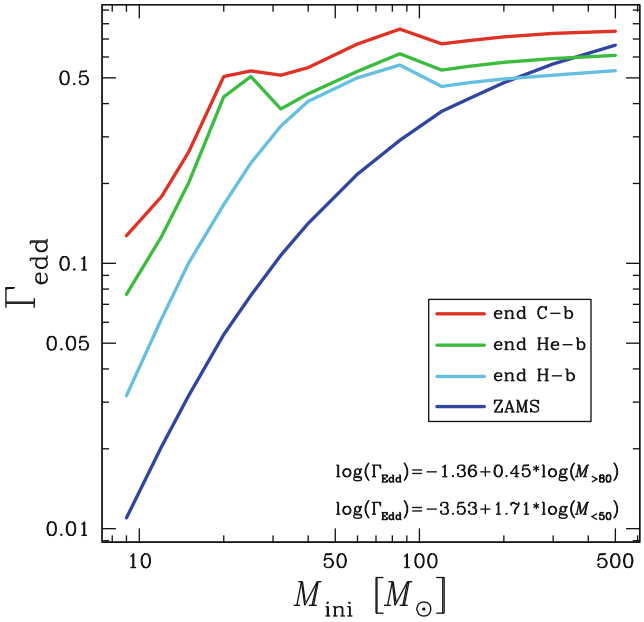

Fig. 7 Eddington parameter, $\Gamma_{\rm edd}$, for rotating models at solar metallicity. $\Gamma_{\rm edd}$ is plotted on the ZAMS (*blue line*) and the end of H- (*light blue*), He- (*green*), and C-burning (*red*) phases. Except for the 300 and 500 $M_\odot$ models, $\Gamma_{\rm edd}$ increases throughout the evolution. At solar metallicity, the highest value (close to 0.8) is actually reached by the 85 $M_\odot$ model at the end of its evolution. This could lead to significant mass loss shortly before the final explosion in a model that ends as a WR star and potentially explain supernova surrounded by a thick circumstellar material without the need for the star to be in the luminous variable phase. The formulae in the *bottom right corner* are linear fits for the mass ranges: 9–50 $M_\odot$ and 80–500 $M_\odot$. The non-rotating models have very similar properties on the ZAMS

a star will produce and may be a reason why the explosion of VMS may look like as if they had happened in an environment similar to those observed around luminous blue variable. The second case is at low metallicity, as highlighted by the 150 $M_\odot$ model at SMC metallicity. Indeed, values above 0.7 are reached before the end of the MS (square symbol). Mass loss prescriptions such as the ones of Vink et al. (2011) and Maeder et al. (2012) may thus play an important role in the fate of VMS. The non-rotating model has a different mass loss history (see Fig. 6), which explains the slightly different evolution of $\Gamma_{\rm Edd}$ near the end of the main sequence.

3.6 Evolution of the Surface Velocity

The surface velocity of stars is affected by several processes. Contraction or expansion of the surface respectively increases and decreases the surface velocity due to the conservation of angular momentum. Mass loss removes angular momentum and

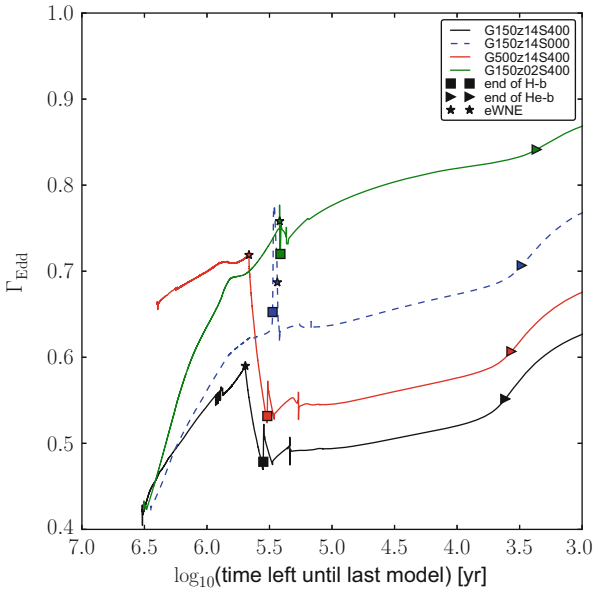

Fig. 8 Evolution of the Eddington parameter, $\Gamma_{\rm Edd}$, as a function of time left until last model (log scale) for the rotating 500 $M_\odot$ model (*solid red*), the rotating 150 $M_\odot$ model (*solid black*), the non-rotating (*dashed*) 150 $M_\odot$ model at solar metallicity, and the rotating 150 $M_\odot$ model at SMC metallicity (*solid green*). The stars indicate the start of the eWNE phase. The *squares* and *triangles* indicate the end of H-b. and He-b. phases, respectively

thus decreases the surface velocity. Finally internal transport of angular momentum generally increases the surface velocity. As shown in Fig. 9 (left panel), at solar metallicity, the surface velocity rapidly decreases during the main sequence due to the strong mass loss over the entire mass range of VMS. At SMC metallicity, mass loss is weaker than at solar metallicity and internal transport of angular momentum initially dominates over mass loss and the surface velocity increases during the first half of the MS phase. During this time, the ratio of surface velocity to critical velocity also increases up to values close to 0.7 (note that the models presented include the effect of the luminosity of the star when determining the critical rotation as described in Maeder and Meynet 2000). However, as the evolution proceeds, the luminosity increases and mass loss eventually starts to dominate and the surface velocity and its ratio to critical rotation both decrease for the rest of the evolution. SMC stars thus never reach critical rotation. The situation at very low and zero metallicities has been studied by several groups (see Chatzopoulos and Wheeler 2012; Ekström et al. 2008; Hirschi 2007; Yoon et al. 2012, and references therein). If mass loss becomes negligible, then the surface velocity reaches critical rotation for a large fraction of the lifetime of the star, which probably leads to mechanical mass loss along the equator. The angular momentum content in the core of VMS stars is discussed further in Sect. 5.4.

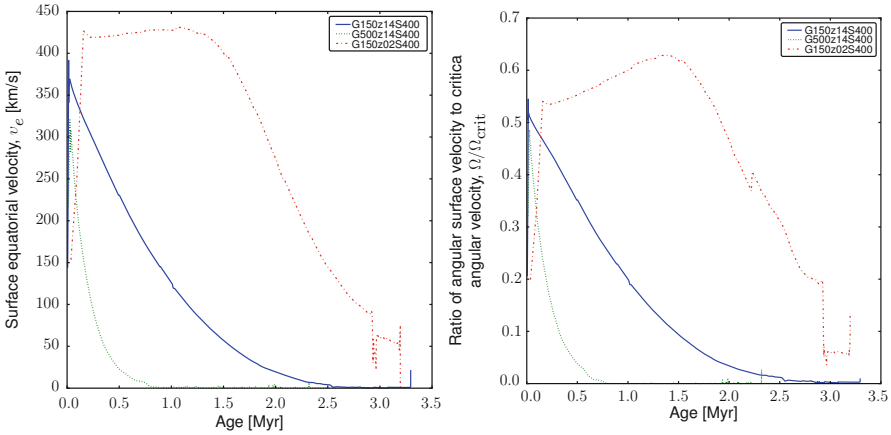

Fig. 9 Evolution of surface equatorial velocity (*left*) and ratio of the surface angular velocity to the critical angular velocity (*right*) for the rotating solar metallicity 150 and 500 $M_\odot$ and SMC 150 $M_\odot$ models as a function of the age of the star

4 WR Stars from VMS

Figure 10 presents the evolution of the surface abundances as a function of the total mass for the solar metallicity rotating models of 150 and 60 $M_\odot$. This figure shows how the combined effects of mass loss and internal mixing change their surface composition. Qualitatively there are no big differences between the 60 and 150 $M_\odot$ models. Since the 150 $M_\odot$ has larger cores, the transition to the various WR stages occurs at larger total masses compared to the 60 $M_\odot$ model. It thus confirms the general idea that a more massive (thus more luminous) WR star originates from a more massive O-type star. Figure 10 shows that all abundances and abundance ratios are very similar for a given WR phase. It is therefore not easy to distinguish a WR originating from a VMS from its surface chemical composition (however see below).

At solar metallicity, the WR phase of non-rotating stellar models for masses between 150 and 500 $M_\odot$ covers between 16% and 38% of the total stellar lifetime. This is a significantly larger proportion than for masses between 20 and 120 $M_\odot$, where the WR phase covers only 0–13% of the total stellar lifetimes. At the LMC metallicity, the proportion of the total stellar lifetime spent as a WR phase for VMS decreases to values between 12% (150 $M_\odot$) and 25% (500 $M_\odot$).

Figure 11 shows how these lifetimes vary as a function of mass for non-rotating and rotating solar metallicity models. Looking first at the non-rotating models (Fig. 11, *left*), we see that the very massive stars (above 150 $M_\odot$) have WR lifetimes between 0.4 and nearly 1 Myr. The longest WR phase is the WNL phase since these stars spend a large fraction of H-burning in this phase. The duration of the

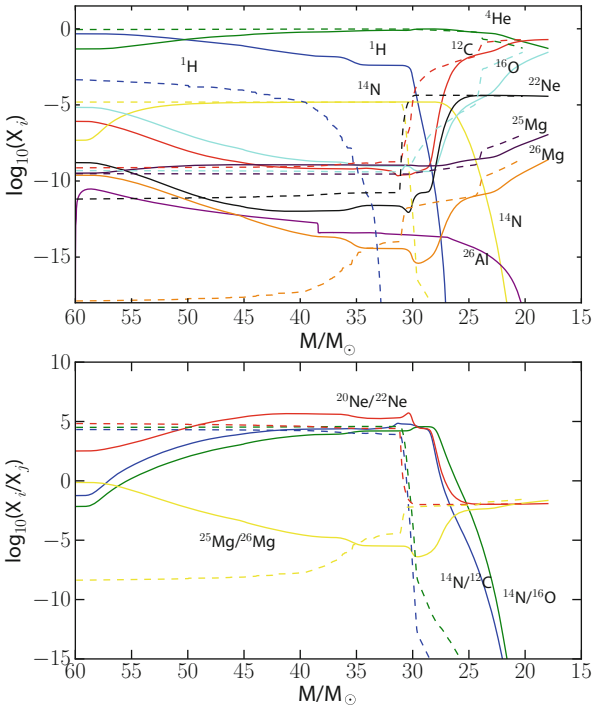

Fig. 10 Evolution of surface abundances of the 150 $M_{\odot}$ (*solid*) and 60 $M_{\odot}$ (*dashed*) rotating solar Z models as a function of total mass (evolution goes from left to right since mass loss peels off the star and reduces the total mass). The *top panel* shows individual abundances, while the *bottom panel* shows abundance ratios

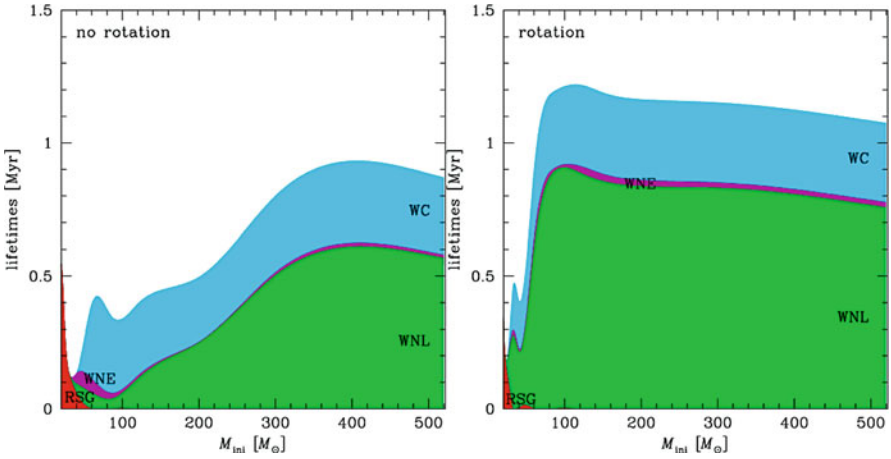

Fig. 11 Lifetimes of the RSG phase and of the different WR phases for the solar metallicity non-rotating (*left*) and rotating (*right*) models. Lifetimes are piled up. For example, the lifetime of the WNE phase extent corresponds to the height of the purple area

WC phases of VMS is not so much different from those of stars in the mass range between 50 and 120 $M_\odot$.

Rotation significantly increases the WR lifetimes. Typically, the WR phase of rotating stellar models for masses between 150 and 500 $M_\odot$ covers between 36 and 43% of the total stellar lifetime. The increase is more important for the lower-mass range plotted in the figures. This reflects the fact that for lower initial mass stars, mass loss rates are weaker and thus the mixing induced by rotation has a greater impact. We see that this increase is mostly due to longer durations for the WNL phase, the WC phase duration remaining more or less constant for the whole mass range between 50 and 500 $M_\odot$ as was the case for the non-rotating models. Rotation has qualitatively similar effects at the LMC and SMC metallicities.

Would the account of the VMS stars in the computation of the number ratios of WR to O-type stars and on the WN/WC ratios have a significant effect? The inclusion of VMS is marginal at solar metallicity, since the durations are only affected by a factor 2. Convoluted with the weighting of the initial mass function (IMF), WR stars originating from VMS only represent ∼10% of the whole population of WR stars (using a Salpeter 1955, IMF) originating from single stars. However, the situation is different at SMC metallicity. Due to the weakness of the stellar winds, single stellar models below 120 $M_\odot$ at this Z do not produce any WC or WO stars (Georgy et al. 2013). In that case, we expect that the few WC/WO stars observed at low metallicity come from VMS or from the binary channel (Eldridge

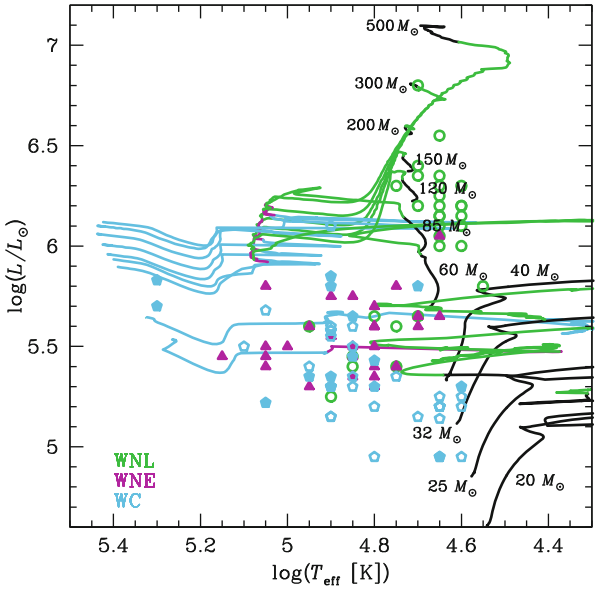

Fig. 12 The positions of WR stars observed by Hamann et al. (2006) and Sander et al. (2012) are indicated with the rotating evolutionary tracks taken from Ekström et al. (2012) for masses up to 120 $M_\odot$ and from Yusof et al. (2013) for VMS

et al. 2008). In starburst regions, the detection of WR stars at very young ages would also be an indication that they come from VMS, as these stars enter the WR phase before their less massive counterparts, and well before WRs coming from the binary channel.

We see in Fig. 12 that VMS models well fit the most luminous WNL stars. On the other hand, they predict very luminous WC stars. Of course the fact that no such luminous WC stars has ever been observed can simply come from the fact that such stars are very rare and the lifetime in the WC phase is moreover relatively short.

5 Late Evolution, Fate, and Remnants of Very Massive Stars

Several studies (Bond et al. 1984; Chatzopoulos and Wheeler 2012; Dessart et al. 2013; Heger and Woosley 2002) have simulated explosions of VMS. Most studies find that VMS ending their life with a carbon-oxygen (CO) core mass between roughly 60 and 130 $M_{\odot}$ explode as pair-instability supernova (PISN, also known as pair-creation SN, PCSN). Whether or not a star produces a PISN can thus be reasonably estimated from the mass of its final CO core, even if their prior evolution is different. In this section, we will thus use the CO core mass to estimate the fate of the models discussed in the previous sections. Note that for lower-mass massive stars ($\lesssim$50 $M_{\odot}$), the CO core mass alone is not sufficient to predict the fate of the star, and other factors like compactness, rotation, and the central carbon abundance at the end of helium burning also play a role (see, e.g., Chieffi and Limongi 2013). More information about VMS and their final explosions can be found in the VMS book (Vink 2015).

5.1 Advanced Phases, Final Masses, and Masses of Carbon-Oxygen Cores

In Fig. 13, the structure evolution diagrams are drawn as a function of the log of the time left until the last model calculated (as opposed to age in Fig. 2). This choice of x-axis allows one to see the evolution of the structure during the advanced stages. In the *left* panel, we can see that, at solar metallicity, VMS have an advanced evolution identical to 40–60 $M_{\odot}$ stars (see, e.g., Fig. 12 in Hirschi et al. 2004) with a radiative core C-burning followed by a large convective C-burning shell, radiative neon burning, and convective oxygen and silicon burning stages. All the solar metallicity models will eventually undergo core collapse after going through the usual advanced burning stages. The central mass fraction of ^{12}C at the start of carbon burning is very low in all VMS models and is anti-correlated with the total mass at the end of helium burning: the higher the total mass, the lower the central ^{12}C mass fraction. This is due to the higher temperature in more massive cores leading to a more efficient $^{12}C(\alpha,\gamma)^{16}O$ relative to 3α.

The similarities between VMS and 40–60 $M_{\odot}$ stars at solar metallicity during the advanced stages can also be seen in the central temperature versus central

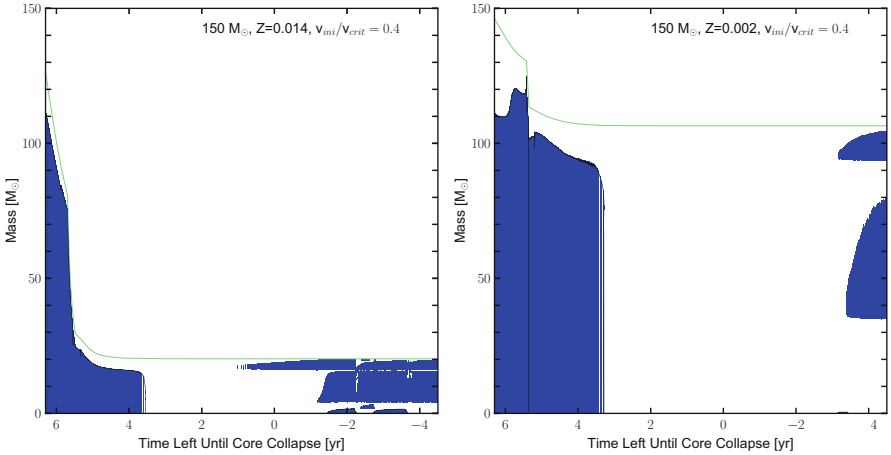

Fig. 13 Structure evolution diagram for rotating 150 $M_\odot$ at solar (*left*) and SMC (*right*) metallicities as a function of the log of the time left until the last model. The *blue zones* represent the convective regions and the *top solid line* the total mass

density diagram (see Fig. 14). Even the evolution of the 500 $M_\odot$ rotating model is close to that of the 60 $M_\odot$ model. The non-rotating models lose less mass as described above, and thus their evolutionary track is higher (see, e.g., the track for the non-rotating 150 $M_\odot$ model in Fig. 14). Non-rotating models at solar metallicity nevertheless stay clear of the pair-instability region ($\Gamma < 4/3$, where Γ is the adiabatic index) in the center.

The situation is quite different at SMC metallicity (see Fig. 13, *right* panel). Mass loss is weaker and thus the CO core is very large (93.5 $M_\odot$ for this 150 $M_\odot$ model). Such a large core starts the advanced stages in a similar way: radiative core C-burning followed by a large convective C-burning shell and radiative neon burning. The evolution starts to diverge from this point onward. As can be seen in T_c vs ρ_c plot, the SMC 150 $M_\odot$ model enters the pair-instability region. This model will thus have a different final fate from those at solar metallicity (see below).

Figure 15 (see also Table 1) shows the final masses of VMS as a function of the initial masses. All models at solar Z, rotating or not, end with a small fraction of their initial mass due to the strong mass loss they experience. Rotation enhances mass loss by allowing the star to enter the WR phase earlier during the MS (see *top* panels of Fig. 2), and the final mass of non-rotating models is generally higher than that of rotating models. At low metallicities, due to the metallicity dependence of radiatively driven stellar winds in both O-type stars (Vink et al. 2001) and WR stars (Eldridge and Vink 2006), final masses are larger.

Figure 16 shows how the CO core masses vary as a function of the initial mass, rotation and metallicity. The CO core ($M_{\rm CO}$) is here defined as the core mass for which the mass fraction of C+O is greater than 75%. Since the CO core mass is so close to the total mass, the behavior is the same as for the total mass and for

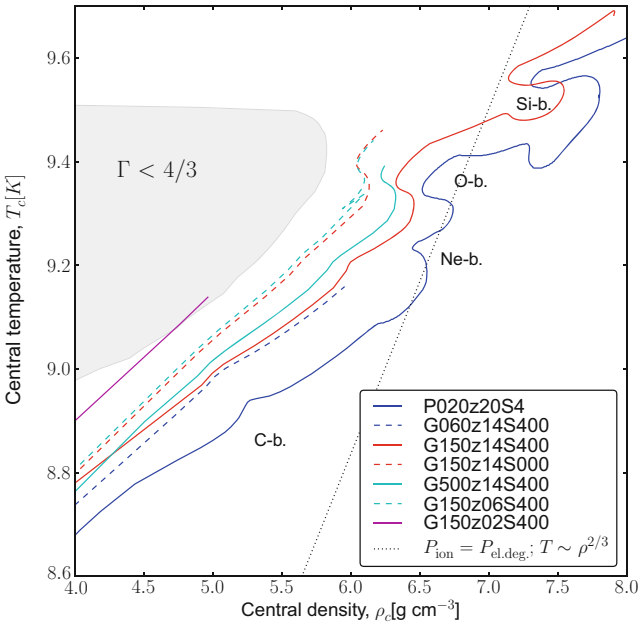

Fig. 14 Evolution of the central temperature T_c versus central density ρ_c for the rotating 20 (From Hirschi et al. 2004), 60 (From Ekström et al. 2012), 150, and 500 $M_\odot$ models and non-rotating 150 $M_\odot$ model at solar metallicity as well as the rotating 150 $M_\odot$ model at SMC metallicity. The *gray shaded area* is the pair-creation instability region ($\Gamma < 4/3$, where Γ is the adiabatic index). The additional *dotted line* corresponds to the limit between nondegenerate and degenerate electron gas

the same reasons. For the rotating solar metallicity models, mass loss is so strong that all models end with roughly the same CO core mass around 20 $M_\odot$. As the metallicity decreases, so does mass loss, and thus the LMC and SMC models have higher final CO core masses and the CO core mass does depend on the initial mass in a monotonous way. Finally, non-rotating models lose less mass than their rotating counterpart since they enter the WR phase later and also have less hot surface. Simulations at $Z = 0.004$ from Yoshida and Umeda (2011) (case A) are also plotted in Fig. 16. The CO core masses they obtain are consistently slightly larger than for the LMC ($Z = 0.006$) models from Yusof et al. (2013).

5.2 Do VMS Produce PISNe?

As mentioned above, the core masses, especially the CO core masses, can be used to estimate whether or not models produce a PISN by using the results of previous studies, which follow the explosion of such massive cores and knowing that VMS with the same CO core masses have similar core evolution from carbon burning

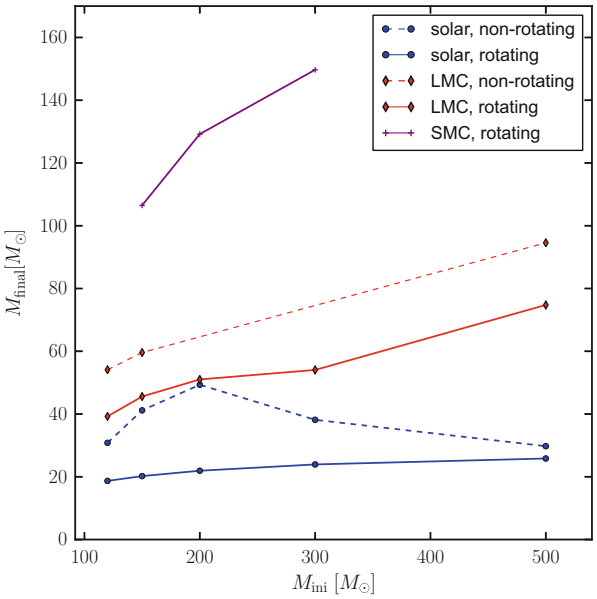

Fig. 15 Final mass versus initial mass for all rotating (*solid lines*) and non-rotating (*dashed line*) models

onward. Heger and Woosley (2002) calculated a grid of models and found that stars with helium cores (M_α) between 64 and 133 $M_\odot$ produce PISNe and that stars with more massive M_α will collapse to a BH without explosion, confirming the results of previous studies, such as Bond et al. (1984). The independent results of Chatzopoulos and Wheeler (2012) also confirm the CO core mass range that produce PISNe.

PISNe occur when very massive stars (VMS) experience an instability in their core during the neon/oxygen burning stage due to the creation of electron-positron pairs out of two photons. The creation of pairs in their oxygen-rich core softens the equation of state, leading to further contraction. This runaway collapse is predicted to produce a very powerful explosion, in excess of 10^{53} erg, disrupting the entire star and leaving no remnant (Bond et al. 1984; Fryer et al. 2001).

Heger and Woosley (2002) also find that stars with M_α between roughly 40 and 63 $M_\odot$ will undergo violent pulsations induced by the pair-instability (PPISNe) leading to strong mass loss but which will not be sufficient to disrupt the core. Thus these stars will eventually undergo core collapse as lower-mass stars. Since in the models at high metallicity presented in this chapter, the CO core masses are very close to M_α (M_α is equal to the final total mass in most models since at high metallicity, all the hydrogen-rich envelope is lost to winds), in this chapter we assume that models will produce a PISN if $60\ M_\odot \lesssim M_{CO} \lesssim 130\ M_\odot$. In Fig. 16, the light gray shaded region corresponds to the zone where one would expect a

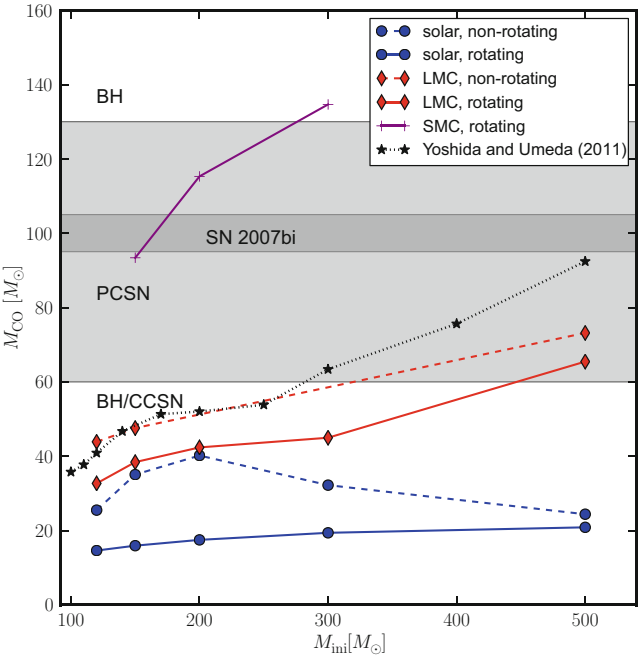

Fig. 16 Mass of carbon-oxygen core of all the models as a function of the initial mass. The *light gray shaded area* represents the range of M_{CO}, for which the estimated fate is a PISN. The *thin dark gray shaded area* corresponds to the estimated M_{CO} of the progenitor of SN 2007bi assuming it is a PISN (see text for more details). The points linked by the *dotted black line* are from the models of Yoshida and Umeda (2011) at $Z = 0.004$, case A

PISN, the dark shaded region showing the estimated range of the carbon-oxygen core of the progenitor of SN 2007bi (see Yusof et al. 2013, for more details).

We see in Fig. 16 that at solar metallicity, none of the models are expected to explode as a PISN. At the metallicity of the LMC, only stars with initial masses above 450 for the rotating models and above about 300 $M_\odot$ for the non-rotating case are expected to explode as a PISN. At the SMC metallicity, the mass range for the PISN progenitors is much more favorable. Extrapolating from the models calculated, all stars in the mass range between about 100 $M_\odot$ and 290 $M_\odot$ could produce PISNe. Thus these models provide support for the occurrence of PISNe in the nearby (not so metal-poor) universe.

Table 2 presents for each of the models, the initial mass ($M_{\rm ini}$), the amount of helium left in the star at the end of the calculation ($M_{\rm He}^{\rm env}$), and final total mass as well as the estimated fate in terms of the explosion type: PISN or core-collapse supernova and black hole formation with or without mass ejection (CCSN/BH). The helium core mass (M_α) is not given since it is always equal to the final total mass, all the models having lost the entire hydrogen-rich layers. Note that some of

Table 2 Initial masses, mass content of helium in the envelope, mass of carbon-oxygen core, final mass in solar masses, and fate of the models estimated from the CO core mass

	Non-rotating				Rotating			
M_{ini}	$M_{\rm He}^{\rm env}$	$M_{\rm co}$	$M_{\rm final}$	Fate	$M_{\rm He}^{\rm env}$	$M_{\rm co}$	$M_{\rm final}$	Fate
Z = 0.014								
120	0.4874	25.478	30.8	CCSN/BH	0.5147	18.414	18.7	CCSN/BH
150	0.6142	35.047	41.2	CCSN/BH	0.5053	19.942	20.2	CCSN/BH
200	0.7765	42.781	49.3	CCSN/BH	0.5101	21.601	21.9	CCSN/BH
300	0.3467	32.204	38.2	CCSN/BH	0.4974	19.468	23.9	CCSN/BH
500	0.3119	24.380	29.8	CCSN/BH	0.5675	20.993	25.8	CCSN/BH
Z = 0.006								
120	1.2289	43.851	54.2	CCSN/BH	0.5665	32.669	39.2	CCSN/BH
150	1.1041	47.562	59.7	CCSN/BH	0.7845	38.436	45.6	CCSN/BH
200	–	–	–	CCSN/BH	0.5055	42.357	51.0	CCSN/BH
300	–	–	–	CCSN/BH	0.5802	44.959	54.0	CCSN/BH
500	1.6428	92.547	94.7	PISN	0.7865	73.145	74.8	PISN
Z = 0.002								
150	–	–	–	–	2.3353	93.468	106.5	PISN
200	–	–	–	–	3.3022	124.329	129.2	PISN
300	–	–	–	–	5.5018	134.869	149.7	BH

these models might experience PPISNe. The reader is referred to Woosley (2017) for more details about PPISNe. Note also that VMS at lower metallicities may retain some hydrogen (see Kozyreva et al. 2017, and references therein).

5.3 Supernova Types Produced by VMS

Let us recall that in VMS convective cores are very large. It is larger than 90% above 200 $M_{\odot}$ at the start of the evolution, and even though it decreases slightly during the evolution, at the end of core H-burning, the convective core occupies more than half of the initial mass in non-rotating models and most of the star in rotating models. This has an important implication concerning the type of supernovae that these VMS will produce. Indeed, even if mass loss is not very strong in SMC models, all the models at SMC metallicity or higher have lost the entire hydrogen-rich layers long before the end of helium burning. Thus the models predict that all VMS stars in the metallicity range presented here will produce either a type Ib or type Ic SN but no type II. At low metallicities (below SMC metallicities) and for not too high masses (between 150 and 200 $M_{\odot}$), VMS may retain some hydrogen and explode as type II PISN, possibly as IIn if a strong mass loss occurs post-helium burning (see Kozyreva et al. 2017, and references therein).

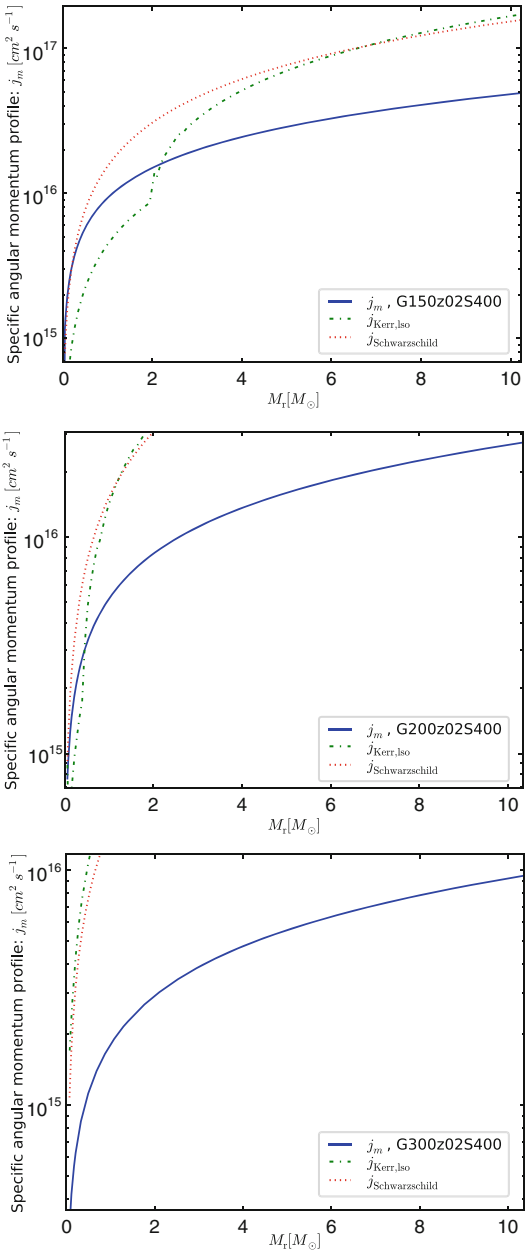

Fig. 17 Specific angular momentum profile, $j_{\rm m}$, as a function of the Lagrangian mass coordinate in the core of the SMC rotating 150, 200, 300 $M_\odot$ models, plotted at the end of the calculations (*solid line*). The *dash-dotted line* is $j_{\rm Kerr,lso} = r_{\rm LSO}\, c$ (Shapiro and Teukolsky 1983, p. 428), where the radius of the last stable orbit, $r_{\rm LSO}$, is given by $r_{\rm ms}$ in formula (12.7.24) from Shapiro and Teukolsky (1983, p. 362) for circular orbit in the Kerr metric. $j_{\rm Kerr,lso}$ is the minimum specific angular momentum necessary to form an accretion disc around a rotating black hole. $j_{\rm Schwarzschild} = \sqrt{12}Gm/c$ (*dotted line*) is the minimum specific angular momentum necessary for a non-rotating black hole, for reference

5.4 GRBs or Magnetars from VMS?

The evolution of the surface velocity was described in Sect. 3.6. Only models at SMC retain a significant amount of rotation during their evolution, but do they retain enough angular momentum for rotation to affect the fate of the star? The angular momentum profile of the SMC models is presented in Fig. 17. Note that the models presented in this section do not include the Tayler-Spruit dynamo to represent the most optimistic (highest possible) prediction concerning the angular momentum in the core of these models. Mass loss in the 300 $M_{\odot}$ model is too strong for the core to retain enough angular momentum for rotation to impact the death of this model. In the 200 $M_{\odot}$ model, and even more so in the 150 $M_{\odot}$ model, however, the central part of the core retains a significant amount of angular momentum that could potentially affect the death of the star. Since the role of rotation is very modest from carbon until just after the end of core silicon burning, even for extremely fast rotators (see, e.g., Chieffi and Limongi 2013; Hirschi et al. 2005), we do not expect rotation to affect significantly the fate of stars that are predicted to explode as PISN during neon-oxygen burning. However, as discussed in Yoon et al. (2012, and references therein), the large angular momentum content is most interesting for the stars that just fall short of the minimum CO core mass for PISN (since fast rotation plays an important role during the early collapse Chieffi and Limongi 2013; O'Connor and Ott 2011; Ott et al. 2004). Indeed, without rotation, these stars would produce a BH following a possible pulsation pair-creation phase, whereas, with rotation, these stars could produce energetic asymmetric explosions (GRBs or magnetars). Since the 150 $M_{\odot}$ model is predicted to explode as a PISN, we thus do not expect the models presented in this section to produce GRBs or magnetars, but such energetic asymmetric explosions are likely to take place in lower-mass and lower metallicity stars (see Hirschi et al. 2005; Woosley and Heger 2006; Yoon and Langer 2005).

Yoon et al. (2012) calculated a grid of zero-metallicity rotating stars, including the Tayler-Spruit dynamo for the interaction between rotation and magnetic fields. They find that fast rotating stars with an initial mass below about 200 $M_{\odot}$ retain enough angular momentum in their cores in order to produce a collapsar ($j > j_{\mathrm{Kerr,lso}}$ see e.g. Woosley 1993) or a magnetar (see, e.g., Burrows et al. 2007; Dessart et al. 2012; Wheeler et al. 2000). Thus some VMS that do not produce PISNe might produce GRBs or magnetars instead.

5.5 Remnants of VMS: Predictions for Black Hole Masses

Table 2 presents for each of the models, the final total mass as well as the estimated fate in terms of the explosion type: PISN or core-collapse supernova and black hole formation with or without mass ejection (CCSN/BH). This table thus gives an estimate of the masses of BHs that VMS produce. These range from about 20 $M_{\odot}$ at solar metallicity to more than 150 $M_{\odot}$ at SMC or lower metallicities. Equally importantly, a gap in the BH mass distribution is expected due to PISNe as well as

the most energetic PPISNe. Woosley (2017) predicts that the gap is roughly between about 50 and 130 $M_{\odot}$. Hopefully gravitational wave detections will be able to test this prediction. So far, the first GW detections have inferred BH masses between 7.5 and 36 $M_{\odot}$ (Abbott et al. 2016a,b,c), which are consistent with these predictions.

6 Supermassive Star Evolution and Fate

Supermassive stars (SMS: $M > 10{,}000\,M_{\odot}$) are usually defined as stars in the mass range $10^{4-6}\,M_{\odot}$. Their formation and existence are much less certain than that of VMS. The two environments, in which they might have formed, are the early universe (Abel et al. 2002b; Stacy et al. 2010) and massive star clusters (Portegies Zwart et al. 2004, 2010). The main interest in SMS comes from the possibility of SMS being progenitors of intermediate-mass and supermassive black holes (IMBH, SMBH, see, e.g., Ohkubo et al. 2006; Rees 1984; Shibata et al. 2016) and also that temperature in SMS is high enough to explain anti-correlations between aluminum and magnesium in globular clusters (Denissenkov and Hartwick 2014; Denissenkov et al. 2015).

Not only the formation process is not well known, but also their mass loss history is unknown since no SMS has ever been observed. Assuming a low enough mass loss, these stars are generally expected to form black holes at the end of their life, final masses being larger than the upper mass limit for PISNe. A low mass loss thus helps the prospect of forming IMBHs or SMBHs. However, even at low metallicities, SMS will evolve close to the Eddington limit so a high mass loss is probable, as is the case for VMS. A high mass loss combined with a very large mass fraction of the convective cores (as discussed above for VMS) facilitates an enrichment of the surrounding ISM with hydrogen-burning products (from helium to aluminum). It is still not easy to explain anti-correlations in clusters. Denissenkov et al. (2015) need to assume that the star gets disrupted in the middle of the main sequence in order to obtain the desired anti-correlations.

Mass loss and the overall stability of the star are major uncertainties for SMS. The kappa or other mechanisms (Baraffe et al. 2001) might lead to fragmentation. Another instability thought to occur in SMS is a general relativistic instability that might lead in a very narrow mass range around 55,000 $M_{\odot}$ to very energetic explosions (see Chen et al. 2014, and references therein). The explosion is triggered by the general relativistic contribution of thermal photons to gravity in the core of the star. This contribution leads to a contraction of the core and explosive helium burning. The fact that the explosion only occurs in a very narrow mass range makes this type of explosions very unlikely (see also the stabilizing effect of rotation in Fowler 1966).

Despite the appeal of considering SMS as progenitors of IMBHs and SMBHs or an explanation for anti-correlations in star clusters, the formation and evolution of SMS is very uncertain, and there is no solid observational evidence for their existence. Their fate is most likely a BH. The mass of the BH could be as low as 10–20 $M_{\odot}$ if mass loss is strong as found for VMS. The BH mass could be much

larger if somehow, at low metallicity, mass loss could remain modest. Note however that these stars evolve close to the Eddington limit so negligible mass loss is not a very realistic assumption for SMS. SMS might, in rare cases, be disrupted via a general relativistic instability if they end their life with a mass around 55,000 $M_{\odot}$. They might also produce, as is predicted for VMS, a PISN if their final mass falls in the range for these explosions (60 $M_{\odot} \lesssim M_{CO} \lesssim$ 130 $M_{\odot}$ Woosley et al. 2002) or PPISNe (40 $M_{\odot} \lesssim M_{CO} \lesssim$ 60 $M_{\odot}$ Woosley 2017).

7 Conclusions

In this chapter, we have discussed the evolution of very massive stars based on stellar evolution models at various metallicities. The main properties of VMS are the following:

- VMS possess very large convective cores during the MS phase. Typically, in a 200 $M_{\odot}$ model on the ZAMS, the convective core extends over more than 90% of the total mass.
- Since the mass-luminosity relation flattens above 20 $M_{\odot}$, VMS have lifetimes that are not very sensitive to their initial mass and range between 2 and 3.5 million years.
- Even in models with no rotation, due to the importance of the convective core, VMS stars evolve nearly chemically homogeneously.
- Most of the very massive stars (all at solar Z) remain in blue regions of the HR diagram and do not go through a luminous blue variable phase.
- They all enter into the WR phase and their typical evolution is Of - WNL- WNE - WC/WO.
- Due to increasing mass loss rates with the mass, very different initial mass stars end with similar final masses. As a consequence, very different initial masses may during some of their evolutionary phases occupy very similar positions in the HRD.
- A significant proportion of the total stellar lifetimes of VMS is spent in the WR phase (about a third).
- At solar metallicity VMS are not expected to explode as PISNe because mass loss rates are too high.
- Whether or not some VMS models retain enough mass to produce a PISN at low metallicity is strongly dependent on mass loss. As discussed above, models that retain enough mass at SMC metallicity (and below) also approach very closely the Eddington limit after helium burning, and this might trigger a strong enough mass loss in order to prevent any VMS from producing a PISN.
- Most VMS lose the entire hydrogen-rich layers long before the end of helium burning. Thus most VMS stars near solar metallicity are expected to produce either a type Ib or type Ic SN but no type II. At low metallicities (below SMC metallicities) and for not too high masses (between 150 and 200 $M_{\odot}$), VMS may

retain some hydrogen and explode as type II PISN, possibly as IIn if a strong mass loss occurs post-helium burning.
- Models near solar metallicity are not expected to produce GRBs or magnetars. The reason for that is that either they lose too much angular momentum by mass loss or they avoid the formation of a neutron star or BH because they explode as PISNe. Lower mass stars at low metallicities ($Z \lesssim 0.002$), however, may retain enough angular momentum as in metal-free stars (see Chatzopoulos and Wheeler 2012; Yoon et al. 2012) for rotation (and magnetic fields) to play a significant role in their explosion.

Even though VMS are rare, their extreme luminosities and mass loss will still contribute significantly to the light and chemistry budget of their host galaxies. And although many VMS will die quietly and form a black hole, some VMS may die as PISNe or GRBs (possibly as magnetars). Thus the extreme properties of VMS compensate for their rarity, and they are worth studying and considering in stellar population and galactic chemical evolution studies. As discussed above, the main uncertainty that strongly affects their evolution and their fate is the uncertainty in mass loss, especially for stars near the Eddington limit. Thus, although the discussions and conclusions presented in this chapter will remain qualitatively valid, quantitative results will change as our knowledge of mass loss in these extreme stars improves.

Supermassive stars (SMS: $M > 10{,}000\,M_{\odot}$) might be the progenitors of intermediate-mass or supermassive black holes or explain anti-correlations in specific abundance ratios in star clusters. In rare circumstances they might explode due to a general relativistic instability. SMS formation and their evolution, however, are very uncertain and there is no solid evidence for their existence. If they exist, SMS evolve close to the Eddington limit, and thus their mass loss is probably very strong and possibly makes their fate similar to VMS.

8 Cross-References

- ▸ Electron Capture Supernovae from Super Asymptotic Giant Branch Stars
- ▸ Influence of Non-spherical Initial Stellar Structure on the Core-Collapse Supernova Mechanism
- ▸ Nucleosynthesis in Hypernovae Associated with Gamma Ray Bursts
- ▸ Nucleosynthesis in Spherical Explosion Models of Core-Collapse Supernovae
- ▸ Population Synthesis of Massive Close Binary Evolution
- ▸ Pre-Supernova Evolution and Nucleosynthesis in Massive Stars and Their Stellar Wind Contribution
- ▸ Supernovae from Massive Stars
- ▸ Supernovae from Rotating Stars

Acknowledgements The author thanks his collaborators at the University of Geneva (C. Georgy, G. Meynet, A. Maeder, and S. Ekström) and Malaysia (N. Yusof) for their significant contributions

to the results presented in this chapter. He acknowledges support from the World Premier International Research Center Initiative (WPI Initiative), MEXT, Japan, and from the ChETEC COST Action (CA16117), supported by COST (European Cooperation in Science and Technology). The research leading to these results has received funding from the European Research Council under the European Union's Seventh Framework Program (FP/2007-2013) / ERC Grant Agreement n. 306901.

References

Abbott BP, Abbott R, Abbott TD, Abernathy MR, Acernese F, Ackley K, Adams C, Adams T, Addesso P, Adhikari RX et al (2016a) Astrophysical implications of the binary black-hole merger GW150914. Astrophys J Lett 818:L22. doi:10.3847/2041-8205/818/2/L22, 1602.03846

Abbott BP, Abbott R, Abbott TD, Abernathy MR, Acernese F, Ackley K, Adams C, Adams T, Addesso P, Adhikari RX et al (2016b) GW151226: observation of gravitational waves from a 22-solar-mass binary black hole coalescence. Phys Rev Lett 116(24):241103. doi:10.1103/PhysRevLett.116.241103, 1606.04855

Abbott BP, Abbott R, Abbott TD, Abernathy MR, Acernese F, Ackley K, Adams C, Adams T, Addesso P, Adhikari RX et al (2016c) Observation of gravitational waves from a binary black hole merger. Phys Rev Lett 116(6):061102. doi:10.1103/PhysRevLett.116.061102, 1602.03837

Abel T, Bryan GL, Norman ML (2002a) The formation of the first star in the universe. Science 295:93–98. doi:10.1126/science.295.5552.93, arXiv:astro-ph/0112088

Abel T, Bryan GL, Norman ML (2002b) The formation of the first star in the universe. Science 295:93–98. doi:10.1126/science.1063991

Baraffe I, Heger A, Woosley SE (2001) On the stability of very massive primordial stars. Astrophys J 550:890–896. doi:10.1086/319808, astro-ph/0009410

Bennett ME, Hirschi R, Pignatari M, Diehl S, Fryer C, Herwig F, Hungerford A, Nomoto K, Rockefeller G, Timmes FX, Wiescher M (2012) The effect of $^{12}C + ^{12}C$ rate uncertainties on the evolution and nucleosynthesis of massive stars. Mon Not R Astron Soc 420:3047–3070. doi:10.1111/j.1365-2966.2012.20193.x, 1201.1225

Bond JR, Arnett WD, Carr BJ (1984) The evolution and fate of very massive objects. Astrophys J 280:825–847. doi:10.1086/162057

Bromm V, Coppi PS, Larson RB (1999) Forming the first stars in the universe: the fragmentation of primordial gas. Astrophys J Lett 527:L5–L8. doi:10.1086/312385, arXiv:astro-ph/9910224

Burrows A, Dessart L, Livne E, Ott CD, Murphy J (2007) Simulations of magnetically driven supernova and hypernova explosions in the context of rapid rotation. Astrophys J 664:416–434. doi:10.1086/519161, arXiv:astro-ph/0702539

Chatzopoulos E, Wheeler JC (2012) Effects of rotation on the minimum mass of primordial progenitors of pair-instability supernovae. Astrophys J 748:42. doi:10.1088/0004-637X/748/1/42, 1201.1328

Chen KJ, Heger A, Woosley S, Almgren A, Whalen DJ, Johnson JL (2014) The general relativistic instability supernova of a supermassive population III star. Astrophys J 790:162. doi:10.1088/0004-637X/790/2/162, 1402.4777

Chieffi A, Limongi M (2013) Pre-supernova evolution of rotating solar metallicity stars in the mass range 13–120 Mo and their explosive yields. Astrophys J 764:21. doi:10.1088/0004-637X/764/1/21

Christlieb N, Bessell MS, Beers TC, Gustafsson B, Korn A, Barklem PS, Karlsson T, Mizuno-Wiedner M, Rossi S (2002) A stellar relic from the early milky way. Nature 419:904–906. doi:10.1038/nature01142, arXiv:astro-ph/0211274

Crowther PA (2001) Stellar winds from massive stars. In: Vanbeveren D (ed) The influence of binaries on stellar population studies, astrophysics and space science library, vol 264. Springer, p 215. ISBN:0792371046, arXiv:astro-ph/0010581

Crowther PA, Schnurr O, Hirschi R, Yusof N, Parker RJ, Goodwin SP, Kassim HA (2010) The R136 star cluster hosts several stars whose individual masses greatly exceed the accepted 150 Mo stellar mass limit. Mon Not R Astron Soc 408:731–751. doi:10.1111/j.1365-2966.2010.17167.x, 1007.3284

Crowther PA, Hirschi R, Walborn NR, Yusof N (2012) Very massive stars and the Eddington limit. In: Drissen L, Rubert C, St-Louis N, Moffat AFJ (eds) Proceedings of a Scientific Meeting in Honor of Anthony F. J. Moffat. Astronomical society of the pacific conference series, vol 465, p 196, 1209.6157

de Jager C, Nieuwenhuijzen H, van der Hucht KA (1988) Mass loss rates in the Hertzsprung-Russell diagram. Astron Astrophys Suppl 72:259–289

Denissenkov PA, Hartwick FDA (2014) Supermassive stars as a source of abundance anomalies of proton-capture elements in globular clusters. Mon Not R Astron Soc 437:L21–L25. doi:10.1093/mnrasl/slt133, 1305.5975

Denissenkov PA, VandenBerg DA, Hartwick FDA, Herwig F, Weiss A, Paxton B (2015) The primordial and evolutionary abundance variations in globular-cluster stars: a problem with two unknowns. Mon Not R Astron Soc 448:3314–3324. doi:10.1093/mnras/stv211, 1409.1193

Dessart L, O'Connor E, Ott CD (2012) The arduous journey to black hole formation in potential gamma-ray burst progenitors. Astrophys J 754:76. doi:10.1088/0004-637X/754/1/76, 1203.1926

Dessart L, Waldman R, Livne E, Hillier DJ, Blondin S (2013) Radiative properties of pair-instability supernova explosions. Mon Not R Astron Soc 428:3227–3251. doi:10.1093/mnras/sts269, 1210.6163

Eggenberger P, Meynet G, Maeder A, Hirschi R, Charbonnel C, Talon S, Ekström S (2007) The Geneva stellar evolution code. Astrophys Space Sci 263. doi:10.1007/s10509-007-9511-y

Ekström S, Meynet G, Chiappini C, Hirschi R, Maeder A (2008) Effects of rotation on the evolution of primordial stars. Astron Astrophys 489:685–698. doi:10.1051/0004-6361:200809633, 0807.0573

Ekström S, Georgy C, Eggenberger P, Meynet G, Mowlavi N, Wyttenbach A, Granada A, Decressin T, Hirschi R, Frischknecht U, Charbonnel C, Maeder A (2012) Grids of stellar models with rotation. I. Models from 0.8 to 120 solar masses at solar metallicity (Z = 0.014). Astron Astrophys 537:A146. doi:10.1051/0004-6361/201117751, 1110.5049

Eldridge JJ, Vink JS (2006) Implications of the metallicity dependence of Wolf-Rayet winds. Astron Astrophys 452:295–301. doi:10.1051/0004-6361:20065001, arXiv:astro-ph/0603188

Eldridge JJ, Izzard RG, Tout CA (2008) The effect of massive binaries on stellar populations and supernova progenitors. Mon Not R Astron Soc 384:1109–1118. doi:10.1111/j.1365-2966.2007.12738.x, 0711.3079

Figer DF (2005) An upper limit to the masses of stars. Nature 434:192–194

Fowler WA (1966) The stability of supermassive stars. Astrophys J 144:180. doi:10.1086/148594

Frebel A, Aoki W, Christlieb N (2005) Nucleosynthetic signatures of the first stars. Nature 434:871–873. doi:10.1038/nature03455

Fryer CL, Woosley SE, Heger A (2001) Pair-instability supernovae, gravity waves, and gamma-ray transients. Astrophys J 550:372–382. doi:10.1086/319719, arXiv:astro-ph/0007176

Georgy C, Ekström S, Meynet G, Massey P, Levesque EM, Hirschi R, Eggenberger P, Maeder A (2012) Grids of stellar models with rotation. II. WR populations and supernovae/GRB progenitors at Z = 0.014. Astron Astrophys 542:A29. doi:10.1051/0004-6361/201118340, 1203.5243

Georgy C, Ekström S, Eggenberger P, Meynet G, Haemmerlé L, Maeder A, Granada A, Groh JH, Hirschi R, Mowlavi N, Yusof N, Charbonnel C, Decressin T, Barblan F (2013) Grids of stellar models with rotation. III. Models from 0.8 to 120 $M_{\text{Ł}}$ at a metallicity Z = 0.002. Astron Astrophys 558:A103. doi:10.1051/0004-6361/201322178, 1308.2914

Gräfener G, Hamann WR (2008) Mass loss from late-type WN stars and its Z-dependence. Very massive stars approaching the Eddington limit. Astron Astrophys 482:945–960. doi:10.1051/0004-6361:20066176, 0803.0866

Greif TH, Glover SCO, Bromm V, Klessen RS (2010) The first galaxies: chemical enrichment, mixing, and star formation. Astrophys J 716:510–520. doi:10.1088/0004-637X/716/1/510, 1003.0472

Hamann WR, Gräfener G, Liermann A (2006) The galactic WN stars. Spectral analyses with line-blanketed model atmospheres versus stellar evolution models with and without rotation. Astron Astrophys 457:1015–1031. doi:10.1051/0004-6361:20065052. arXiv:astro-ph/0608078

Heger A, Woosley SE (2002) The nucleosynthetic signature of population III. Astrophys J 567:532–543. doi:10.1086/338487, arXiv:astro-ph/0107037

Hirschi R (2007) Very low-metallicity massive stars: pre-SN evolution models and primary nitrogen production. Astron Astrophys 461:571–583. doi:10.1051/0004-6361:20065356, arXiv:astro-ph/0608170

Hirschi R, Meynet G, Maeder A (2004) Stellar evolution with rotation. XII. Pre-supernova models. Astron Astrophys 425:649–670. doi:10.1051/0004-6361:20041095, astro-ph/0406552

Hirschi R, Meynet G, Maeder A (2005) Stellar evolution with rotation. XIII. Predicted GRB rates at various Z. Astron Astrophys 443:581–591. doi:10.1051/0004-6361:20053329, arXiv:astro-ph/0507343

Kippenhahn R, Weigert A (1990) Stellar structure and evolution. Springer, Berlin

Kozyreva A, Gilmer M, Hirschi R, Fröhlich C, Blinnikov S, Wollaeger RT, Noebauer UM, van Rossum DR, Heger A, Even WP, Waldman R, Tolstov A, Chatzopoulos E, Sorokina E (2017) Fast evolving pair-instability supernova models: evolution, explosion, light curves. Mon Not R Astron Soc 464:2854–2865. doi:10.1093/mnras/stw2562, 1610.01086

Krumholz MR (2015) The formation of very massive stars. In: Vink JS (ed) Very massive stars in the local universe. Astrophysics and space science library, vol 412. Springer International Publishing, p 43. doi:10.1007/978-3-319-09596-7_3, 1403.3417

Maeder A (1980) The most massive stars in the galaxy and the LMC – quasi-homogeneous evolution, time-averaged mass loss rates and mass limits. Astron Astrophys 92: 101–110

Maeder A, Meynet G (2000) Stellar evolution with rotation. VI. The Eddington and Omega-limits, the rotational mass loss for OB and LBV stars. Astron Astrophys 361:159–166

Maeder A, Georgy C, Meynet G, Ekström S (2012) On the Eddington limit and Wolf-Rayet stars. Astron Astrophys 539:A110. doi:10.1051/0004-6361/201118328, 1201.5013

Muijres LE, de Koter A, Vink JS, Krtička J, Kubát J, Langer N (2011) Predictions of the effect of clumping on the wind properties of O-type stars. Astron Astrophys 526:A32. doi:10.1051/0004-6361/201014290

Nugis T, Lamers HJGLM (2000) Mass-loss rates of Wolf-Rayet stars as a function of stellar parameters. Astron Astrophys 360:227–244

O'Connor E, Ott CD (2011) Black hole formation in failing core-collapse supernovae. Astrophys J 730:70. doi:10.1088/0004-637X/730/2/70, 1010.5550

Oey MS, Clarke CJ (2005) Statistical confirmation of a stellar upper mass limit. Astrophys J Lett 620:L43–L46. doi:10.1086/428396, arXiv:astro-ph/0501135

Ohkubo T, Umeda H, Maeda K, Nomoto K, Suzuki T, Tsuruta S, Rees MJ (2006) Core-collapse very massive stars: evolution, explosion, and nucleosynthesis of population III 500–1000 M_{solar} stars. Astrophys J 645:1352–1372. doi:10.1086/504578, astro-ph/0507593

Ott CD, Burrows A, Livne E, Walder R (2004) Gravitational waves from axisymmetric, rotating stellar core collapse. Astrophys J 600:834–864. doi:10.1086/379822, arXiv:astro-ph/0307472

Owocki SP (2015) Instabilities in the envelopes and winds of very massive stars. In: Vink JS (ed) Very massive stars in the local universe. Astrophysics and space science library, vol 412. Springer International Publishing, p 113. doi:10.1007/978-3-319-09596-7_5, 1403.6745

Portegies Zwart SF, Baumgardt H, Hut P, Makino J, McMillan SLW (2004) Formation of massive black holes through runaway collisions in dense young star clusters. Nature 428:724–726. doi:10.1038/nature02448, astro-ph/0402622

Portegies Zwart SF, McMillan SLW, Gieles M (2010) Young massive star clusters. ARA&A 48:431–493. doi:10.1146/annurev-astro-081309-130834, 1002.1961

Rees MJ (1984) Black hole models for active galactic nuclei. ARA&A 22:471–506. doi:10.1146/annurev.aa.22.090184.002351

Salpeter EE (1955) The luminosity function and stellar evolution. Astrophys J 121:161. doi:10.1086/145971

Sander A, Hamann WR, Todt H (2012) The galactic WC stars. Stellar parameters from spectral analyses indicate a new evolutionary sequence. Astron Astrophys 540:A144. doi:10.1051/0004-6361/201117830, 1201.6354

Schneider FRN, Izzard RG, de Mink SE, Langer N, Stolte A, de Koter A, Gvaramadze VV, Hußmann B, Liermann A, Sana H (2014) Ages of young star clusters, massive blue stragglers, and the upper mass limit of stars: analyzing age-dependent stellar mass functions. Astrophys J 780:117. doi:10.1088/0004-637X/780/2/117, 1312.0607

Shapiro SL, Teukolsky SA (1983) Black holes, white dwarfs, and neutron stars: the physics of compact objects. Research supported by the National Science Foundation. Wiley-Interscience, New York, p 663

Shibata M, Sekiguchi Y, Uchida H, Umeda H (2016) Gravitational waves from supermassive stars collapsing to a supermassive black hole. PhysRevD 94(2):021501. doi:10.1103/PhysRevD.94.021501, 1606.07147

Stacy A, Greif TH, Bromm V (2010) The first stars: formation of binaries and small multiple systems. Mon Not R Astron Soc 403:45–60. doi:10.1111/j.1365-2966.2009.16113.x, 0908.0712

Sylvester RJ, Skinner CJ, Barlow MJ (1998) Silicate and hydrocarbon emission from galactic M supergiants. Mon Not R Astron Soc 301:1083–1094. doi:10.1046/j.1365-8711.1998.02078.x

Umeda H, Nomoto K (2002) Nucleosynthesis of zinc and iron peak elements in population III type II supernovae: comparison with abundances of very metal poor halo stars. Astrophys J 565:385–404. doi:10.1086/323946

van Loon JT, Groenewegen MAT, de Koter A, Trams NR, Waters LBFM, Zijlstra AA, Whitelock PA, Loup C (1999) Mass-loss rates and luminosity functions of dust-enshrouded AGB stars and red supergiants in the LMC. Astron Astrophys 351:559–572, arXiv:astro-ph/9909416

Vink JS (ed) (2015) Very massive stars in the local universe, astrophysics and space science library, vol 412. Springer International Publishing. doi:10.1007/978-3-319-09596-7, 1406.4836

Vink JS, de Koter A, Lamers HJGLM (2001) Mass-loss predictions for O and B stars as a function of metallicity. Astron Astrophys 369:574–588. doi:10.1051/0004-6361:20010127, arXiv:astro-ph/0101509

Vink JS, Muijres LE, Anthonisse B, de Koter A, Gräfener G, Langer N (2011) Wind modelling of very massive stars up to 300 solar masses. Astron Astrophys 531:A132. doi:10.1051/0004-6361/201116614, 1105.0556

Wheeler JC, Yi I, Höflich P, Wang L (2000) Asymmetric supernovae, pulsars, magnetars, and gamma-ray bursts. Astrophys J 537:810–823. doi:10.1086/309055, arXiv:astro-ph/9909293

Woosley SE (1993) Gamma-ray bursts from stellar mass accretion disks around black holes. Astrophys J 405:273–277

Woosley SE (2017) Pulsational pair-instability supernovae. Astrophys J 836:244. doi:10.3847/1538-4357/836/2/244, 1608.08939

Woosley SE, Heger A (2006) The progenitor stars of gamma-ray bursts. Astrophys J 637:914–921. doi:10.1086/498500

Woosley SE, Heger A, Weaver TA (2002) The evolution and explosion of massive stars. Rev Mod Phys 74:1015–1071

Yoon SC, Langer N (2005) Evolution of rapidly rotating metal-poor massive stars towards gamma-ray bursts. Astron Astrophys 443:643–648. doi:10.1051/0004-6361:20054030

Yoon SC, Dierks A, Langer N (2012) Evolution of massive population III stars with rotation and magnetic fields. Astron Astrophys 542:A113. doi:10.1051/0004-6361/201117769, 1201.2364

Yoshida T, Umeda H (2011) A progenitor for the extremely luminous Type Ic supernova 2007bi. Mon Not R Astron Soc 412:L78–L82. doi:10.1111/j.1745-3933.2011.01008.x, 1101.0635

Yusof N, Hirschi R, Meynet G, Crowther PA, Ekström S, Frischknecht U, Georgy C, Abu Kassim H, Schnurr O (2013) Evolution and fate of very massive stars. Mon Not R Astron Soc 433:1114–1132. doi:10.1093/mnras/stt794, 1305.2099